Materials Science & Engineering A 614 (2014) 6–15

Contents lists available at ScienceDirect

Materials Science & Engineering A

journal homepage: www.elsevier.com/locate/msea

Influence of water cooling on microstructure and mechanical properties of friction stir welded 2014Al-T6 joints

Z. Zhang, B.L. Xiao, Z.Y. Ma *

Shenyang National Laboratory for Materials Science, Institute of Metal Research, Chinese Academy of Science, 72 Wenhua Road, Shenyang 110016, China

ARTICLE INFO

Article history:
Received 4 May 2014
Received in revised form
24 June 2014
Accepted 25 June 2014
Available online 2 July 2014

Keywords:
Aluminum alloys
Fiction stir welding
Water cooling
Microstructure
Mechanical properties

ABSTRACT

6 mm thick 2014Al-T6 alloy plates were friction stir welded under both normal air cooling (AC) and submerged water cooling (WC) conditions at welding speeds of 100–800 mm/min and a constant rotational rate of 800 rpm. While sound FSW joints could be produced under the investigated welding speeds of 100–800 mm/min for the AC condition, defect-free joint was only obtained under the low welding speed of 100 mm/min and higher welding speeds of 400–800 mm/min led to void defects or breakdown of welding tools for the WC condition. The FSW thermal cycle resulted in the formation of a low hardness zone (LHZ) on both retreating side and advancing side of the FSW 2014Al-T6 joints for both welding conditions. The LHZs were located at the heat affected zone and the thermo-mechanically affected zone adjacent to the nugget zone for the AC and WC joints, respectively. The tensile strength of the AC joints increased as the welding speed increased from 100 to 800 mm/min. Water cooling did not enhance the hardness of LHZs and tensile strength of FSW 2014Al-T6 joints.

1. Introduction

2014 Aluminum alloy is widely used for aircraft structural applications where damage tolerance and high strength are paramount [1]. However, wide industrial applications are restricted by the process technologies especially welding technology, because 2014Al is unweldable using conventional fusion welding techniques due to its hot cracking sensitivity [2].

Friction stir welding (FSW), a relatively new solid state joining process which uses a non-consumable rotational tool to generate frictional heat at the welding location without material melting, produces defect-free joints and smaller temperature gradient than conventional arc process [3,4]. Thus, FSW is considered an ideal process for joining high strength aerospace 2xxx aluminum alloys [5].

For the 2014Al-T6 alloy, although the FSW joints were reported to have better joint efficiency compared to the fusion welded joints, the gap between the strength values of the base metal (BM) and the FSW joints is still large ($>20\%$) [6]. Heat treatment is the most effective way to improve the mechanical properties of precipitation-hardened aluminum alloys. Zhang et al. [7] reported that while post-weld artificial aging could not improve the mechanical properties of FSW 2014Al-T6 joints, post-weld T6 heat treatment enhanced the tensile strength of the joints to the BM level. However, the fine grains of nugget zone (NZ) grew up abnormally to millimeter-scale after post-weld T6 treatment and crack tended to develop along the "S" line at the bottom of the joints for high welding speed, damaging the mechanical properties of the joints.

For FSW joints of precipitation-hardened aluminum alloys (2xxx, 6xxx and 7xxx), the heat-affected zone (HAZ) is the low hardness zone (LHZ) because of the significant dissolution/coarsening of the precipitates [8–12]. The LHZ plays an important role in determining the mechanical properties and fracture behavior of the FSW joints. Submerged welding is considered an effective method to reduce the degradation of joint performance in the HAZ [13]. Submerged welding refers to the workpieces that are placed in a liquid medium and the FSW process is conducted under a specific ambience.

In recent years, several kinds of Al alloys have been subjected to extensive submerged FSW investigations [13–19]. Benavides et al. [14] reported that liquid nitrogen cooling resulted in a significant reduction of temperature and the formation of a large worm-hole defect in the NZ of FSW 2024Al joint. Upadhyay and Reynolds [15] conducted FSW of 7050Al-T7 alloy under normal air, water (20 °C), and liquid medium (-25 °C) cooling conditions and found that both water and liquid medium cooling enhanced the tensile strength of the FSW 7050Al-T7 joints. Fu et al. [13] conducted FSW of 7050Al-T3 alloy under normal air, cold water (8 °C), and hot water cooling (98 °C) conditions and reported that both cold and hot water cooling improved the tensile strength of the FSW 7050Al-T3 joints.

* Corresponding author. Tel./fax: +86 24 83978908.
E-mail address: zyma@imr.ac.cn (Z.Y. Ma).

http://dx.doi.org/10.1016/j.msea.2014.06.093
0921-5093/

Similarly, Fratini et al. [16] reported that the water cooling (WC) enhanced the tensile strength of FSW 7075Al-T6 joints. Nelson et al. [17] reported that the tensile strength of FSW 7075Al-T7351 joints were improved by 10%, but the tensile strength of FSW 2195Al-T8 joints were minimally affected ($<3\%$ change) under WC condition. Zhang et al. [18] conducted WC FSW of 2219Al-T6 at rotational rates of 600–1400 rpm and found that the void defects were produced when increasing the rotational rate from 1200 to 1400 rpm. Similarly, Liu et al. [19] reported that for WC FSW 2219Al-T6 joints produced at a constant rotational rate of 800 rpm and welding speeds of 50–200 mm/min, increasing the welding speed from 150 to 200 mm/min resulted in the formation of the void defects.

The above investigations indicated that the liquid medium exerted varied effects on the joint quality and tensile properties of FSW joints for different precipitation-hardened aluminum alloys. However, no detailed explanation about the influencing mechanism of rapid cooling on the joint quality and mechanical properties of FSW joints was provided in these studies. Moreover, investigation of submerged FSW 2014Al alloy is lacking.

In this study, the 2014Al-T6 alloy was subjected to FSW investigation at a tool rotational rate of 800 rpm and the welding speeds of 100–800 mm/min under both normal AC and submerged WC conditions. The aim of this work is to (a) explore the possibility to obtain sound submerged FSW 2014Al-T6 joints at varied welding speeds and (b) elucidate the influencing mechanism of WC on the joint quality and mechanical properties of FSW joints.

2. Experimental procedure

6 mm thick commercial 2014Al-T6 rolled plate was used in this study as the BM. The nominal chemical compositions and the tensile properties of the plate were listed in Table 1. The plates, with a length of 300 mm and a width of 90 mm, were butt-welded along the rolling direction with a tool tilt angle of 2.75° using a FSW machine under two different cooling conditions: (a) normal AC without any external thermal conditioning and (b) submerged WC by immersing the plates and welding tools into flowing room temperature water during FSW. A tool with a concave shoulder 20 mm in diameter and a threaded cylindrical pin 8 mm in diameter and 5.8 mm in length was used. The tool was made of H13 tool steel with a hardness of HRC 45.

Three welding parameters were selected by fixing the rotational rate at 800 rpm and increasing the welding speed from 100 to 800 mm/min, as shown in Table 2. The FSW samples were designated in brief forms. For example, sample AC-800-100 denotes the sample welded at a rotational rate of 800 rpm and a welding speed of 100 mm/min under the AC condition. Sample WC-800-100 denotes the sample welded at a rotational rate of 800 rpm and a welding speed of 100 mm/min under the WC condition. All the FSW samples were naturally aged at room temperature for more than 10 days for subsequent microstructural examination, hardness and tension tests.

All the FSW samples were cross sectioned from the joints perpendicular to the welding direction using an electrical discharge machine. Vickers microhardness measurement was conducted on the cross-section perpendicular to the welding direction using an automatic testing machine (LECO, LM-247AT) under a load of 500 g for 13 s. The microhardness profiles were obtained along the mid-thickness of the cross-section of the joints. In order to obtain the hardness distribution maps, a total of five test lines were measured throughout the cross-section at an interval of 1 mm, with a total of 155 indentations. In each line, there were 31 indentations that extended from the weld center to as far as 15 mm on both advancing side (AS) and retreating side (RS).

Metallographic observation was carried out by optical microscopy (OM, Axiovert 200 MAT). The samples for OM were ground and polished and then etched using Keller's reagent (190 ml water, 2 ml hydrofluoric acid, 3 ml hydrochloric acid and 5 ml nitric acid). The precipitate distributions in the as-welded joints were observed by transmission electron microscopy (TEM TECNAI 20). Thin foils for TEM observation, which were cut from corresponding locations in the weld using an electrical-discharge machine, were prepared by jet electropolishing using a solution of 70 pct methanol and 30 pct nitric at 243 K (-30 °C) and 19 V. Much care was taken to ensure location-to-location correspondence between the observations and hardness measurements.

In order to obtain the real mechanical properties and fracture locations of the FSW joints, the joint surfaces of tensile specimens were planed with abrasive paper to insure an equal cross-sectional area at various locations of the FSW joints. The configuration and size of the transverse tensile specimens are shown in Fig. 1. Room-temperature tensile tests were carried out at a strain rate of $6\times10^{-4}\ s^{-1}$ and the tensile properties of each sample reported were averages of three test results.

3. Results

3.1. Joint quality

Fig. 2 shows the surfacial morphologies of the FSW 2014Al-T6 joints under various welding conditions. Under the AC condition with a rotational rate of 800 rpm, the joint surface of sample

Table 1
Chemical compositions and mechanical properties of 2014Al-T6 rolled plate.

Chemical composition								Mechanical properties	
Cu	Mg	Mn	Fe	Si	Zn	Ti	Al	YS, MPa	UTS, MPa
3.9–5.0	0.2–0.8	0.4–1.2	0.7	0.5–1.2	0.25	0.15	Bal.	430	470

Table 2
Welding parameters of FSW 2014Al-T6 joints.

Sample	Cooling conditions	Rotational rate, rpm	Travel speed, mm/min	Designation
1	Air cooling	800	100	AC-800-100
		800	400	AC-800-400
		800	800	AC-800-800
2	Water cooling	800	100	WC-800-100
		800	400	WC-800-400
		800	800	WC-800-800

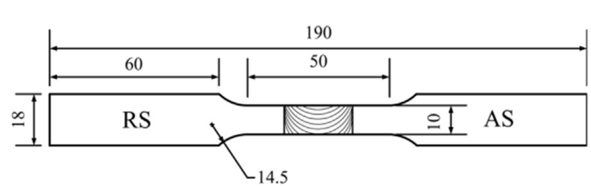

Fig. 1. Configuration and size of tensile specimen.

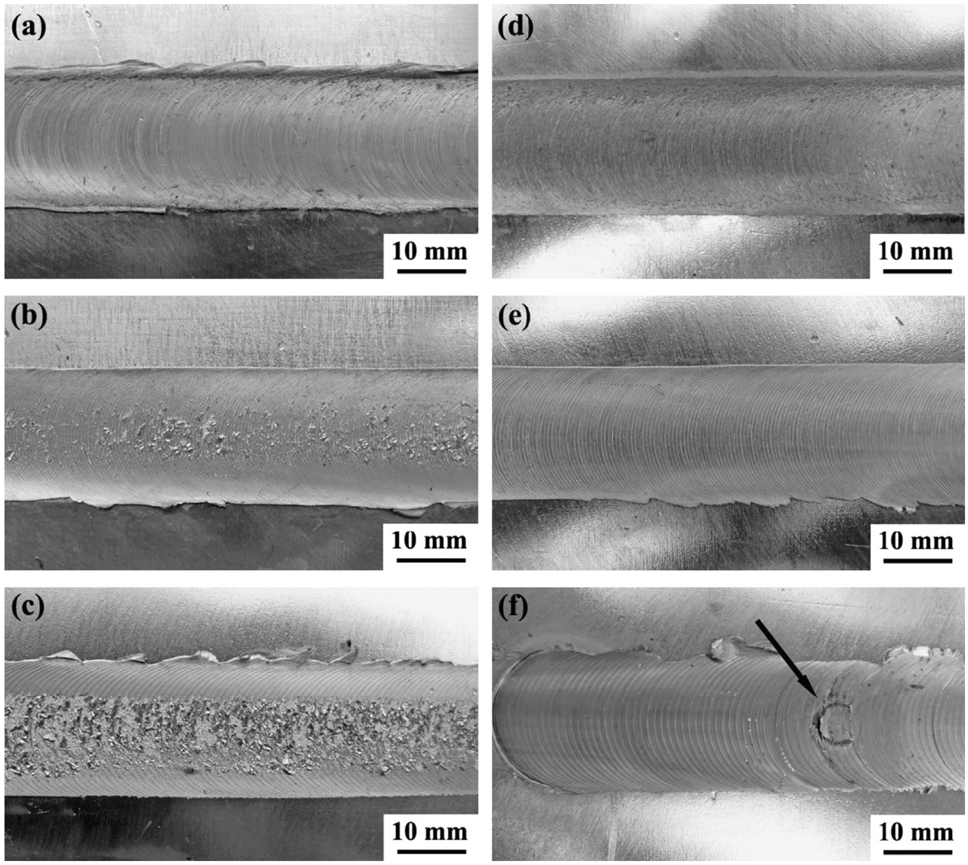

Fig. 2. Surfacial morphologies of FSW 2014Al-T6 joints: (a) AC-800-100, (b) AC-800-400, (c) AC-800-800, (d) WC-800-100, (e) WC-800-400, and (f) WC-800-800.

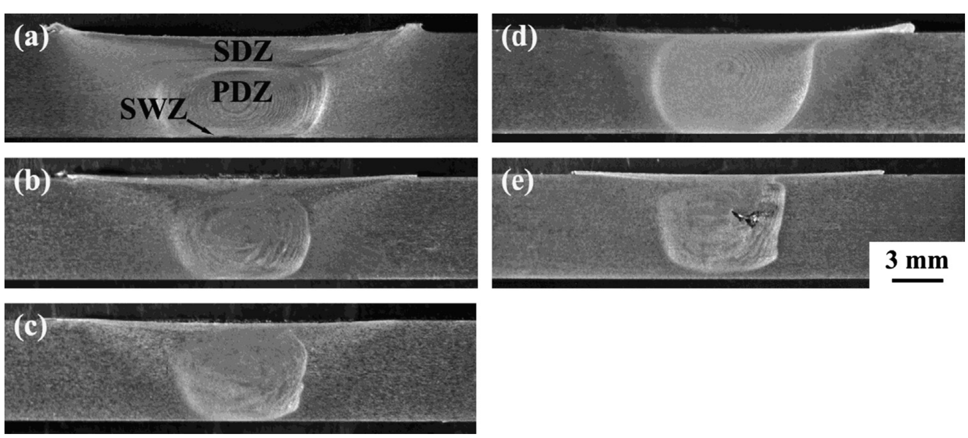

Fig. 3. Cross-sectional macrostructures of FSW 2014Al-T6 joints: (a) AC-800-100, (b) AC-800-400, (c) AC-800-800, (d) WC-800-100, and (e) WC-800-400 (the AS is on the right).

AC-800-100 was smooth (Fig. 2a). When increasing the welding speed from 100 to 400 mm/min, a slight surface delamination was observed on the joint surface of sample AC-800-400 (Fig. 2b). When further increasing the welding speed from 400 to 800 mm/min, the joint surface of sample AC-800-800 exhibited a severe surface delamination (Fig. 2c). In contrast, the joint surfaces of the WC FSW joints were smooth under welding speeds of 100 and 400 mm/min (Figs. 2d and f). However, the pin was broken down under a high welding speed of 800 mm/min (marked by the black arrow in Fig. 2f).

Fig. 3 shows the macrostructures on the transverse cross-sections of the FSW 2014Al-T6 joints. For the AC FSW joints, no welding defect was detected at the investigated welding speeds of 100–800 mm/min (Fig. 3a–c). For the WC FSW joints, sound FSW joint was obtained only at the low welding speed of 100 mm/min (Fig. 3d), with increasing the welding speed from 100 to 400 mm/min, obvious void defects were observed in the sample WC-800-400 (Fig. 3e). According to the role of shoulder and pin in the formation of the NZ, the NZ can be subdivided into three sub-zones: the shoulder-driven zone (SDZ), the pin-driven zone (PDZ) and the swirl zone (SWZ) [20–22], as shown in Fig. 3a. It can be seen that a comparatively large PDZ with regular onion ring structures and a narrow SDZ were observed in the sample AC-800-100 (Fig. 3a). However, only a PDZ with reduced size and

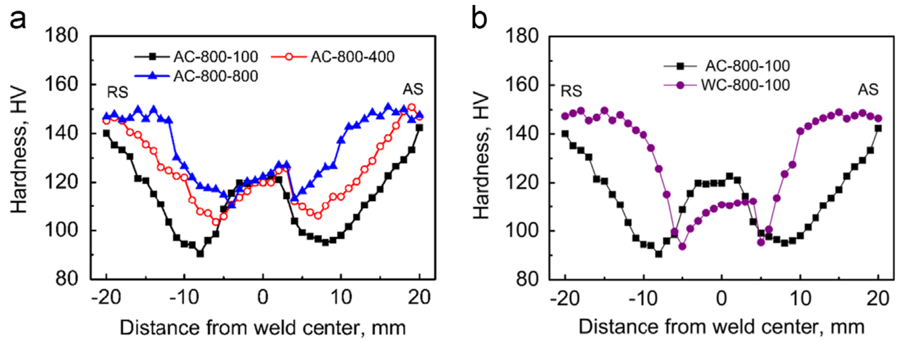

Fig. 4. Microhardness profiles of FSW 2014Al-T6 joints showing effect of (a) welding speed under normal welding condition, and (b) water cooling.

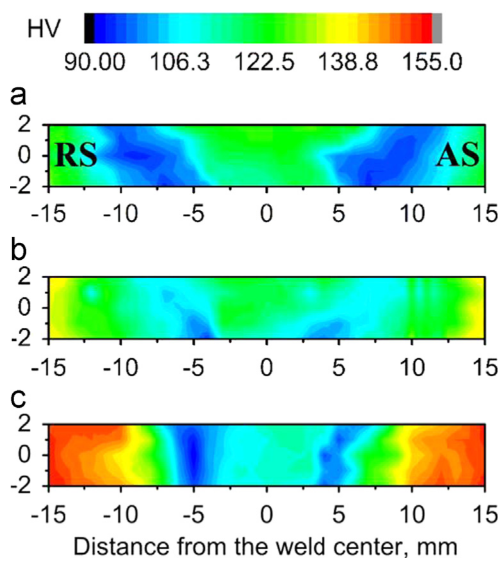

Fig. 5. Microhardness contour maps of (a) sample AC-800-100, (b) sample AC-800-400, and (c) sample WC-800-100.

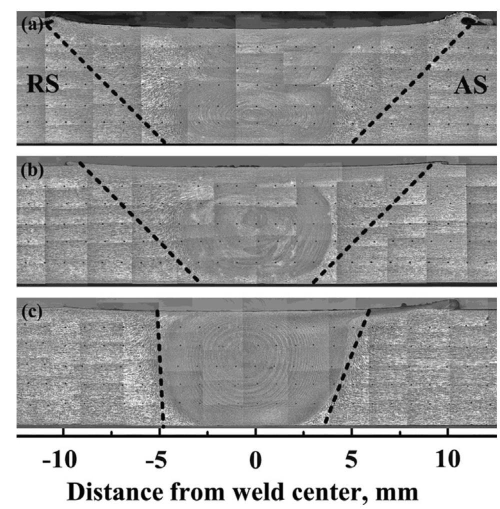

Fig. 6. Location of LHZs (marked by the black dotted line) of (a) sample AC-800-100, (b) sample AC-800-400, and (c) sample WC-800-100.

irregular onion ring structures was observed in samples AC-800-400 and AC-800-800 (Figs. 3b and c). Moreover, only a large PDZ was observed in sample WC-800-100 (Fig. 3d).

3.2. Microhardness map

The effects of the welding speed and water cooling on the hardness profiles of the FSW 2014Al-T6 joints are shown in Fig. 4a and b. All the hardness profiles exhibited a "W" shape with a low hardness zone (LHZ) on both AS and RS of the FSW joints and the hardness of the NZ was lower than that of the BM. At a constant rotational rate of 800 rpm, increasing the welding speed from 100 to 800 mm/min enhanced the hardness values of the LHZs and moved their position towards the weld center (Fig. 4a). The water cooling exerted no noticeable influence on the hardness values of the LHZs but moved the position of the LHZs towards the weld center (Fig. 4b). Furthermore, the water cooling reduced the hardness of the NZ.

It should be pointed out that the above single hardness profile could not determine the fracture path of the FSW 2014Al-T6 joints because of limited lowest hardness points. In order to accurately predict the fracture behavior of the FSW 2014Al-T6 joints, the microhardness contour maps and the macrographs with the hardness test points of samples AC-800-100, AC-800-400, and WC-800-100 are shown in Figs. 5 and 6, respectively. For sample AC-800-100, two LHZs were clearly observed on both the RS and the AS (Fig. 5a). It can be determined that the LHZ was located at the HAZ and was about a $\sim 45^{\circ}$ angle to the tensile axis (marked with dotted lines in Fig. 6a). With the increase in the welding speed from 100 to 400 mm/min, while the location of the LHZ for sample AC-800-400 was similar to that for sample AC-800-100 (Fig. 6b), the hardness of the LHZ for sample AC-800-400 increased significantly (Fig. 5b). Compared with that for sample AC-800-100, the hardness decreased in the NZ and was essentially unchanged in the LHZs for sample WC-800-100 (Fig. 5c). However, the LHZ for sample WC-800-100 was located at the thermo-mechanically affected zone (TMAZ) adjacent to the NZ and was almost vertical to the tensile axis, as shown in Figs. 5c and 6c by dotted lines.

3.3. Microstructure

Fig. 7a–d shows the OM micrographs of the BM, NZ, TMAZ (RS) and HAZ (RS) of sample AC-800-100. It can be seen that the elongated grains of the BM resulting from the rolling process were 100–200 μm long and approximately 20–60 μm wide (Fig. 7a). In the NZ, the microstructure was characterized by the fine and equiaxed recrystallized grains (about 10 μm) arising from the severe plastic deformation and thermal exposure during welding (Fig. 7b). The upward elongated grains were observed in the TMAZ (Fig. 7c), which underwent less plastic deformation and lower heat input. Thus there was no recrystallization in this zone. Notably coarsened grains were observed in the HAZ (Fig. 7d), at which the

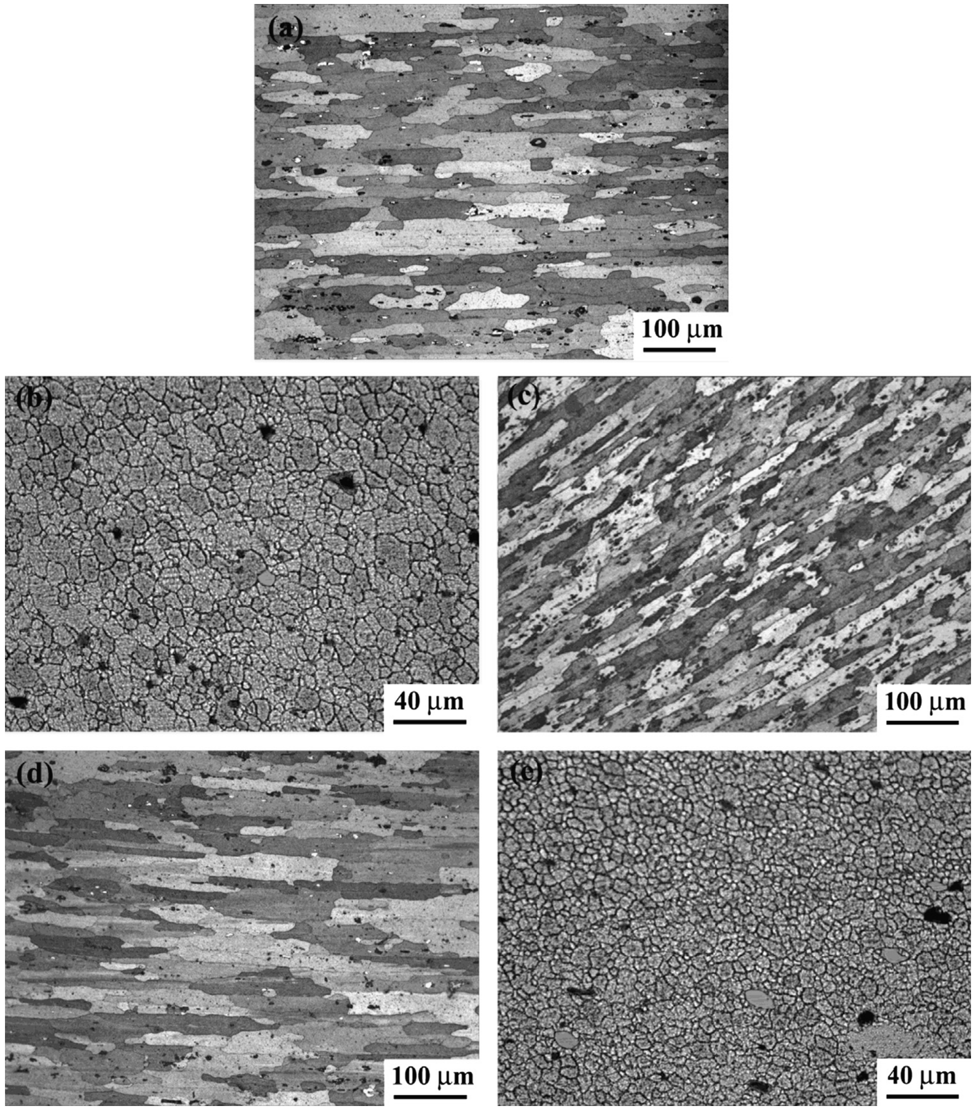

Fig. 7. OM images of (a) BM, (b) NZ, (c) TMAZ and (d) HAZ of sample AC-800-100; (e) NZ of sample WC-800-100.

plastic deformation was absent and only heat input played a role. Fig. 7e shows the OM micrographs of the NZ of sample WC-800-100. It can be seen that the grain size (about 6 μm) of the NZ for sample WC-800-100 was much smaller than that for sample AC-800-100.

Fig. 8 shows the bright-field TEM images of the BM, NZ and LHZ (RS) of samples AC-800-100, AC-800-400, and WC-800-100. The main strengthening precipitates of 2014Al-T6 alloy are needle-shaped Al_2Cu precipitates and rod-shaped Al_2CuMg precipitates. In the BM, the two kinds of precipitates were distributed and were hard to differentiate due to the small size (Fig. 8a). For sample AC-800-100, only few coarsened precipitates were observed in the NZ and the diffraction pattern showed that no GPB zones existed in the NZ (Fig. 8b). In the LHZ, the microstructure was characterized by high density of coarsened and rod-shaped Al_2CuMg phases, and no Al_2Cu phases were observed in this zone (Fig. 8c). For sample AC-800-400, the microstructure characteristic in the NZ was nearly identical to that for sample AC-800-100 (Fig. 8d). Compared with that for sample AC-800-100, the density of coarse Al_2CuMg phases significantly decreased in the LHZ for sample AC-800-400 (Fig. 8e). The microstructure of the NZ and LHZ of sample WC-800-100 was similar to that of sample WC-800-100 (Figs. 8f and g).

3.4. Tensile properties

The tensile strength of the FSW 2014Al-T6 joints is shown in Table 3. Table 3 reveals two important findings. Firstly, for the AC FSW joints under the constant rotational rate of 800 rpm, the tensile strength of the FSW joint largely increased when increasing the welding speed from 100 to 400 mm/min and was only slightly improved with further increasing the welding speed from 400 to 800 mm/min. This is in good agreement with the results of FSW 6061Al-T6 reported by Liu and Ma [9]. Secondly, compared with that of sample AC-800-100, the water cooling did not improve the tensile strength of sample WC-800-100. This is consistent with the variation in the hardness of the LHZs (Fig. 4b).

3.5. Fracture behavior

In order to accurately locate the tensile fracture location of the FSW joints, the cross-sections of failed specimens were etched, as shown in Fig. 9. It can be seen that sample AC-800-100 fractured along the LHZ on the AS (Fig. 9a) and the shear fracture path was $\sim 45^\circ$ angle to the tensile axis, which was in good agreement with the distribution of the LHZ. Similar fracture mode was previously

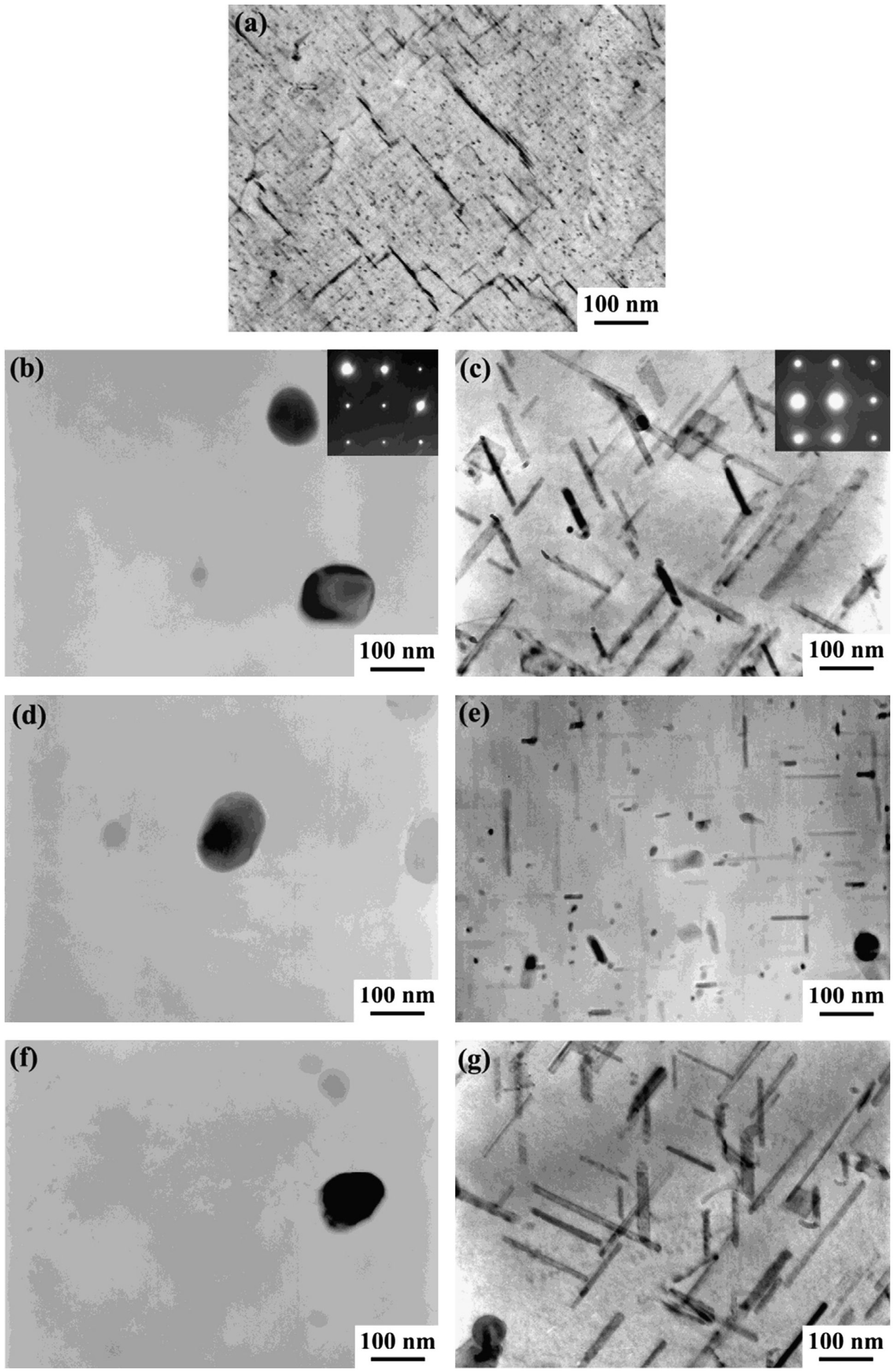

Fig. 8. TEM micrographs and associated diffraction patterns: (a) BM, (b) NZ and (c) LHZ of sample AC-800-100; (d) NZ and (e) LHZ of sample AC-800-400; (f) NZ and (g) LHZ of sample WC-800-100.

Table 3
Transverse tensile properties of FSW 2014Al-T6 joints.

Sample	UTS, MPa	Joint efficiency, %
AC-800-100	366 ± 1	77.5
AC-800-400	404 ± 1	85.5
AC-800-800	416 ± 3	88.0
WC-800-100	369 ± 4	78.0

reported in Refs. [8,9]. The fracture mode of samples AC-800-400 and AC-800-800 was similar to that of sample AC-800-100. However, the fracture location of sample WC-800-100 was not precisely along the LHZ (Fig. 9b).

Figs. 10 and 11 show the typical SEM fractographs of samples AC-800-100 and WC-800-100. The macroscopic image showed that the fracture surface of sample AC-800-100 was flat (Fig. 10a). The magnified image of position A exhibited the mixed fracture

(Fig. 11a), which was in agreement with the fracture characteristic reported in Refs. [8–12]. However, the macroscopic fracture surface of sample WC-800-100 was like a convex platform (Fig. 10b). The magnified image of the top zone (position B) exhibited ductile fracture with dimples (Fig. 10b). The magnified images of the middle zone (position C) and bottom zone (position D) exhibited brittle fracture with steps (Fig. 11c and d).

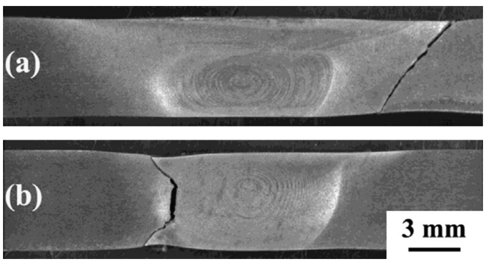

Fig. 9. Fracture locations of (a) sample AC-800-100 and (b) sample WC-800-100 (the AS is on the right).

4. Discussion

4.1. Effect of water cooling on joint quality

During FSW, the joint quality was closely related to the material flow. The welding tool drove the material to flow, forming a flow field. According to the relationship between material flow characteristic and joint quality during FSW, three material flow states were defined in Refs. [22,23]; that is, insufficient material flow, balance material flow and excessive material flow states. The balance material flow state is an ideal welding state without the occurrence of welding defects. It could be obtained by a reasonable combination of rotational rate, welding speed and plunge depth. The defects were easily produced in the insufficient and excess material flow states, which generally resulted from the high welding speed and rotational rate, respectively [23].

The investigated welding parameters and joint quality in the previous studies [14,18,19] and this study are summarized in Table 4. In the previous studies and this study, the sound FSW joints were obtained at a wide range of rotational rate and welding speed for the AC condition but at a comparatively narrow range of

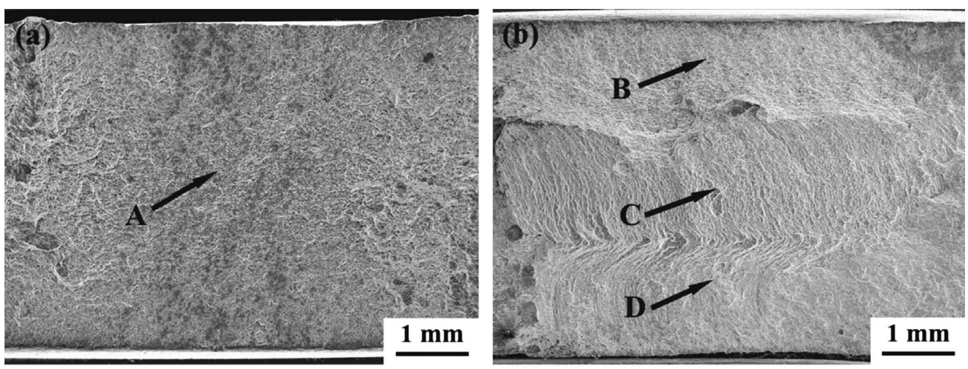

Fig. 10. Fractographs of (a) sample AC-800-100 and (b) sample WC-800-100.

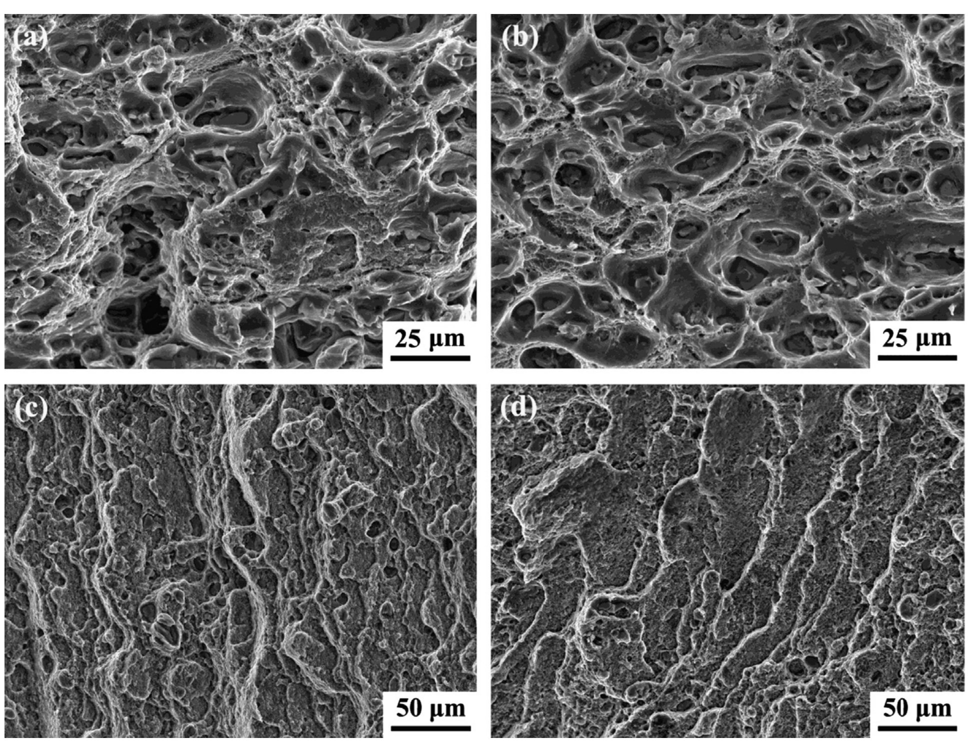

Fig. 11. Magnified micrographs: (a–d) correspond positions A–D in Fig. 10(a) and (b).

Table 4
A summary of welding parameters and joint quality of submerged FSW joints of various aluminum alloys.

BM	Plate thickness, mm	Cooling condition	Rotational rate, rpm	Welding speed, mm/min	Defective sample	Refs.
2014Al-T6	6.0	Air cooling Water cooling	800	100–800	Non 800-400 800-800	This study
2024Al	6.5	Air cooling Liquid nitrogen cooling	650	60	Non 650-60	[14]
2219Al-T6	7.5	Water cooling	600–1400	100	1400-100	[18]
2219Al-T6	7.5	Water cooling	800	50–200	800-200	[19]

Table 5
A summary of tensile strength of FSW joints of various aluminum alloys.

BM	Plate thickness, mm	Cooling condition	Max UTS_{FSW}, MPa	Joint efficiency, %	Refs.
2014Al-T6	6.0	Air cooling	366	78	This study
		Water cooling	369	79	
7050Al	5.5	Air cooling	325	82	[13]
		Water cooling	340	86	
7050Al-T7451	6.35	Air cooling	515	98	[15]
		Water cooling	535	105	
7075Al-T6	3.0	Air cooling	356	81	[16]
		Water cooling	382	87	
2195Al-T8	6.5	Air cooling	410	71	[17]
		Water cooling	420	73	
7075Al-T7351	9.53	Air cooling	405	80	
		Water cooling	450	89	

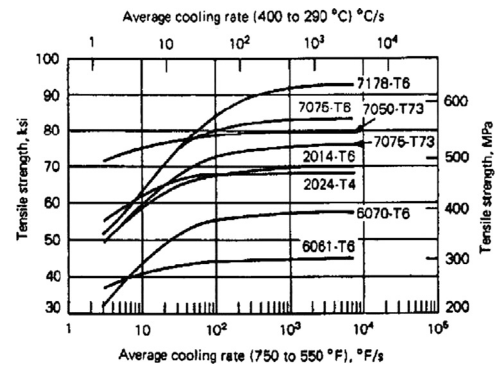

Fig. 12. Tensile strength of aluminum alloys as a function of average cooling rate during quenching [17].

rotational rate and welding speed for the WC condition. This could be explained as follows, with focus on the present FSW 2014Al-T6 joints.

In this study, under the AC condition, the balance material flow state could be easily obtained under the welding speed of 100 mm/min for the rotational rate of 800 rpm, sound FSW joints were therefore produced (Figs. 2a and 3a). Increasing the welding speed from 100 to 400 and 800 mm/min tended to change the material flow state from balance to insufficiency due to inadequate material flow [23]. However, this trend could be avoided by properly increasing the plunge depth for the FSW 2014Al-T6 joints. The sound FSW 2014Al-T6 joints were therefore achieved at higher welding speeds of 400 and 800 mm/min (Figs. 2b and c, and 3b and c).

The water cooling sharply increased the FSW heating and cooling rates and decreased the heat input, weakening the material flow in the NZ. This easily caused the insufficient material flow. Under the low welding speed of 100 mm/min for the rotational rate of 800 rpm, the weakening role of water cooling narrowed the size of the NZ and did not result in defect because the balance material flow state could be obtained by increasing the plunge depth (Figs. 2d and 3d). However, with increasing the welding speed from 100 to 400 mm/min, water cooling resulted in the material flow state changing from balance to insufficiency, which could not be avoided by increasing the plunge depth. The void defects were therefore produced in sample WC-800-400 (Fig. 3e). When further increasing the welding speed from 400 to 800 mm/min, the degree of insufficiency state became much more serious, resulting in the breakdown of pin during FSW (Fig. 2f).

It should be noted that the material flow is closely related to the plastic deformation ability of the BM. Under rapid cooling condition, the easily deformed aluminum alloys can generally be welded at comparatively wider range of welding parameters than the hard deformed aluminum alloys. Moreover, the welding tool is also an important influential aspect for the joint quality. The high temperature alloy is thought to have better high temperature performance than that of carbon steel and may allow higher welding speed and plunge depth.

4.2. *Effect of water cooling on microstructure and mechanical properties*

The effect of water cooling on tensile strength of the FSW precipitation-hardened aluminum alloys in Refs. [13,15–17] and this study are summarized in Table 5. For different aluminum alloys, water cooling exhibited distinctly different effects on the tensile strength of FSW joints. The water cooling largely improved the tensile strength of the FSW joints of 7075Al and 7050Al alloys [13,15–17]. However, for 2195Al-T8 alloy in Ref. [17] and 2014Al-T6 alloy in this study, the water cooling minimally enhanced the tensile strength of the FSW joints.

Nelson et al. [17] reported that the effect of water cooling on the mechanical properties of FSW joint was associated with the quench sensitivity of aluminum alloys. The effects of quench rates from elevated temperatures on the tensile properties of aluminum alloys are shown in Fig. 12. The quench sensitive aluminum alloys (such as 7075Al alloy) exhibit abrupt changes in the tensile strength with the quench rate, while the tensile strength of the less quench sensitive aluminum alloys (such as 2195Al [17] and 2014Al alloy) vary slowly. These are consistent with the variation of tensile strength for submerged FSW joints of 7075Al, 2195Al and 2014Al alloy. However, this could not explain the change in the tensile strength of FSW 7050Al alloy in Refs. [13,15] because 7050Al alloy is a less quench sensitive alloy. This indicates that there exist some other factors influencing the role of water cooling in the FSW process.

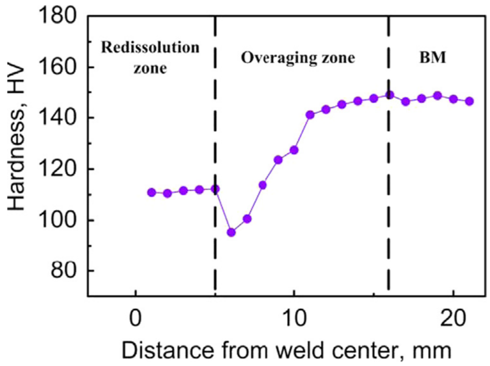

Fig. 13. Schematic diagram showing two sub-zones on transverse cross-section of FSW 2014Al-T6 joints (sample WC-800-400).

For the FSW precipitation-hardened aluminum alloys, their fracture behavior and mechanical properties were mainly dependent on the distribution of the LHZs, which were closely related to the precipitate distribution of the FSW joints. Based on the correlation of the precipitate evolution and the hardness distribution, two sub-zones can be named on the transverse cross-section of the FSW 2014Al-T6 joints, as shown in Fig. 13, that is, dissolution zone and overaging zone, respectively.

The severe plastic deformation and high heat input resulted in the dissolution of most of the Al_2Cu and Al_2CuMg precipitates as well as the coarsening of few remaining Al_2Cu and Al_2CuMg precipitates in the NZ (Fig. 8b, d and f), which was named the dissolution zone. Possibly because the cooling process of FSW eliminated the vacancies, strongly slowing down the formation of the GP and GPB zones at room temperature after welding, the GP and GPB zones did not form in the NZ during the subsequent natural aging (Fig. 8b, d and f). Several investigations showed that, for precipitation-hardened aluminum alloys, the formation of solute clusters, verified by atom probe tomography (APT) technology, could improve the hardness [23–26]. During the subsequent natural aging, it was very likely that the solute clusters formed in the NZ of FSW 2014Al-T6 joints. Thus, the hardness of the NZ (about 110–120 HV) is higher than that of solution treated 2014Al alloy (about 50–60 HV) (Fig. 4a). Under the WC condition, water cooling reduced the heat input and the degree of solid solution of solutes in the NZ, therefore the average microhardness of the NZ of sample WC-800-100 was lower than that of sample AC-800-100, despite smaller grain size for sample WC-800-100 (Fig. 7b and e).

The TMAZ and HAZ correspond to the overaging zone, which experienced the thermal cycles with the peak temperatures between 200 and 410 °C [27,28], resulting in over-aging, that is, the coarsening of the Al_2Cu and Al_2CuMg precipitates in this study. Based on temperature measurement and microstructural examinations in the LHZs of FSW 6061Al-T6 joints, Liu and Ma [9] proposed an isothermal dissolution layer layers (ITDLs) model that all the LHZs experienced the thermal cycles with the same peak temperature of 360–370 °C. The ITDLs model was verified by numerical simulation and also proved to be suited for the FSW joints of other precipitation-hardened aluminum alloys [29,30]. The peak temperatures of thermal cycles in the ITDLs were about 340–360 °C for FSW 2014Al-T6 joints [31], 300 °C for FSW 7075Al-T6 joints [12] and 280 °C for FSW 7050Al-T6 joints [13]. As a result, the positions of the LHZs varied for the FSW joints of different precipitation-hardened aluminum alloys. Based on Refs. [12,13,17], the positions of the LHZs relative to the welding tool of the FSW joints under the similar welding conditions are schematically shown in Fig. 14.

It should be pointed out that that the role of water cooling in the FSW process may be associated with positions of the LHZs.

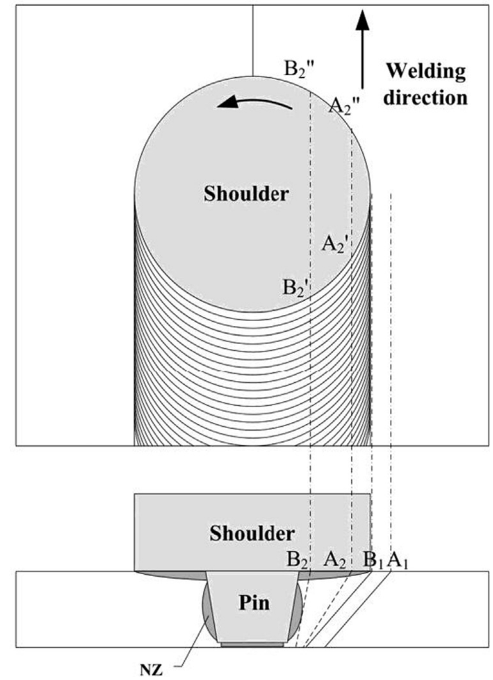

Fig. 14. Schematic positions of LHZs relative to the welding tool for FSW joints of different aluminum alloys.

During FSW, the microstructure deterioration of the LHZs is induced by the friction heat between the plates and welding tool (shoulder and pin). Under the WC condition, the heat input of the zone far from the welding tool was significantly reduced by water, which possesses the larger heat conductivity coefficient and heat capacity than air, while for the zone close to the welding tool, the heat input was less inhibited by water. Increasing the distance between the welding tool and LHZs could strengthen the cooling role of water. For the FSW joints of 7050Al and 7075Al, the LHZs were reported to be beside the shoulder zone and schematically located at position A_1 under the AC condition [12,13,17]. In this case, water exerted a strong forced cooling on the LHZs and moved the LHZs from position A_1 to A_2 (Fig. 14). During this process, the LHZs of the WC FSW joints experienced a short time of direct heating by the welding tool from A_2' to A_2'' and water cooling would shorten the duration above the phase-transition temperatures considerably. This indicates that water cooling led to significantly reduced overaging in LHZs compared to air cooling. Therefore, water cooling improved the mechanical properties of the FSW joints of 7050Al and 7075Al significantly in Refs. [13,15–17]. For the FSW 2014Al-T6 joints, the LHZs were close to the welding tool and located at position B_1 under the AC condition in this study (Figs. 6 and 14). Under the WC condition, water cooling moved the LHZs from position B_1 to B_2, i.e. from the edge towards the center of the shoulder. In this case, the LHZs of the WC FSW joints experienced a long time of direct heating by the shoulder from B_2' to B_2''. In this case, the duration above the phase-transition temperatures was less affected by water. As a consequence, water cooling minimally enhanced the hardness in the LHZs and the tensile strength of sample WC-800-100 in this study (Table 3 and Fig. 4b).

The fracture location of the FSW joints was mainly dependent on the lowest hardness distribution. The LHZs of the AC FSW 2014Al-T6 joints were far from the NZ and were located at the HAZs, in which only high density of coarsened and rod-shaped Al_2CuMg phases and coarsened grains existed. Thus, the AC joints precisely fractured along the LHZs (Fig. 9a). For the WC FSW 2014Al-T6 joints, the LHZs were close to the NZ/TMAZ interface

(Fig. 6c), which is a complex transition zone between the dissolution zone and overaging zone and between the fine grains and the elongated grains. The abrupt change in the precipitates and grain microstructure led to the fracture location of sample WC-800-100 not being precisely along the LHZ (Fig. 9b). The fracture surface of sample WC-800-100 therefore exhibited the varied morphological characteristics at different positions (Figs. 10b and, 11c and d).

The results of this study demonstrate the close relationship between the water cooling, welding parameters, joint quality, and mechanical properties for the FSW 2014Al-T6 joints. Firstly, there are a wide range of welding speeds between 100 and 800 mm/min available for producing defect-free joints for the AC condition. However, only low welding speed was feasible for WC FSW. Secondly, the effect of water cooling on the tensile strength of the FSW joints was related with the position of the LHZs relative to the shoulder. Choosing the proper alloys is necessary for effectively applying the WC welding technology.

5. Conclusions

(1) Sound FSW 2014Al-T6 joints could be obtained under welding speeds of 100–800 mm/min under the air cooling condition. Under the water cooling condition, defect-free FSW joints could only be obtained under a low welding speed of 100 mm/min and high welding speeds of 400–800 mm/min easily resulted in void defects or breakdown of pin.
(2) The FSW thermal cycle resulted in the LHZs on both RS and AS due to the dissolution and coarsening of Al_2Cu and Al_2CuMg precipitates. The hardness of the LHZs increased as the welding speed increased from 100 to 400 and 800 mm/min. Water cooling did not enhance the hardness value of the LHZs but moved the location of LHZs towards the weld center.
(3) The LHZ of the FSW 2014Al-T6 joints was located at the HAZ under the air cooling condition and was located at the TMAZ adjacent to the NZ under the water cooling condition.
(4) The FSW 2014Al-T6 joints fractured along the LHZs on the AS under the air cooling condition but fractured partially along the LHZs under the water cooling condition.
(5) The tensile strength of the FSW 2014Al-T6 joints increased as the welding speed increased from 100 to 800 mm/min under the air cooling condition. Water cooling did not enhance the tensile strength of FSW 2014Al-T6 joints.

Acknowledgments

This work was supported by the National Natural Science Foundation of China under Grant no. 51331008.

References

[1] A. Pakes, G.E. Thompson, P. Skeldon, P.C. Morgan, Corros. Sci. 45 (2003) 1275–1287.
[2] D. Fersini, A. Pirondi, Eng. Fract. Mech. 74 (2007) 468–480.
[3] L. Commin, M. Dumont, J.E. Masse, L. Barrallier, Acta Mater. 57 (2009) 326–334.
[4] R.S. Mishra, Z.Y. Ma, Mater. Sci. Eng. R 50 (2005) 1–78.
[5] M.A. Sutton, B. Yang, A.P. Reynolds, R. Taylor, Mater. Sci. Eng. A. 323 (2002) 160–166.
[6] Y.H. Zhao, S.B. Lin, L. Wu, F.X. Qu, Trans. Nonferr. Met. Soc. China 15 (2005) 1248–1252.
[7] Z. Zhang, B.L. Xiao, Z.Y. Ma, Adv. Mater. Res. 409 (2012) 299–304.
[8] S.R. Ren, Z.Y. Ma, L.Q. Chen, Scr. Mater. 56 (2007) 69–72.
[9] F.C. Liu, Z.Y. Ma, Metall. Mater. Trans. A 39 (2008) 2378–2388.
[10] C.B. Fuller, M.W. Mahoney, M. Calabrese, L. Micona, Mater. Sci. Eng. A 527 (2010) 2233–2240.
[11] R. Brown, W. Tang, A.P. Reynolds, Mater. Sci. Eng. A 115 (2009) 513–514.
[12] M.W. Mahoney, C.G. Rhodes, J.G. Flintoff, R.A. Spurling, W.H. Bingel, Metall. Mater. Trans. A 29 (1998) 1955–1964.
[13] R.D. Fu, Z.Q. Sun, R.C. Sun, Y. Li, H.J. Liu, L. Liu, Mater. Des. 32 (2011) 4825–4831.
[14] S. Benavides, Y. Li, L.E. Murr, D. Brown, J.C. McClure, Scr. Mater. 41 (1999) 809–815.
[15] U. Upadhyay, A.P. Reynolds, Mater. Sci. Eng. A 527 (2010) 1537–1543.
[16] L. Fratini, G. Buffa, R. Shivpuri, Int. J. Adv. Manuf. Technol. 43 (2009) 664–670.
[17] T.W. Nelson, R.J. Steel, W.J. Arbegast, Sci. Technol. Weld. Join. 8 (2003) 283–288.
[18] H.J. Zhang, H.J. Liu, L. Yu, Mater. Des. 32 (2011) 4402–4407.
[19] H.J. Liu, H.J. Zhang, L. Yu, Mater. Des. 32 (2011) 15481553.
[20] K. Kumar, S.V. Kailas, Mater. Sci. Eng. A 485 (2008) 367–374.
[21] W.J. Arbegast, Scr. Mater. 58 (2008) 372–376.
[22] Z. Zhang, B.L. Xiao, D. Wang, Z.Y. Ma, Metall. Mater. Trans. A 42 (2011) 1717–1726.
[23] R.K.W. Marceau, G. Sha, R. Ferragut, A. Dupasquier, S.P. Ringer, Acta Mater. 58 (2010) 4923–4929.
[24] S. Pogatscher, H. Antrekowitsch, H. Leitner, T. Ebner, P.J. Uggowitzer, Acta Mater. 59 (2011) 3352–3363.
[25] T. Marlaud, A. Deschamps, F. Bley, W. Lefebvre, B. Baroux, Acta Mater. 58 (2010) 4814–4826.
[26] Z. Zhang, B.L. Xiao, Z.Y. Ma, Acta Mater. 73 (2014) 227–239.
[27] P.A. Colegrove, H.R. Shercliff, Sci. Technol. Weld. Join. 8 (2003) 360–368.
[28] Y.S. Sato, M. Urata, H. Kokawa, Metall. Mater. Trans. A 33 (2002) 625–635.
[29] X.X. Zhang, B.L. Xiao, Z.Y. Ma, Metall. Mater. Trans. A 42 (2011) 3218–3228.
[30] X.X. Zhang, B.L. Xiao, Z.Y. Ma, Metall. Mater. Trans. A 42 (2011) 3229–3239.
[31] J. Caroline, d.M. Bruno, D. Anne, S. Aude, J. Mater. Process. Technol. 213 (2013) 826–837.